

GRAPH AND HODGE LAPLACIANS: SIMILARITY AND DIFFERENCE

EMILY RIBANDO-GROS, RUI WANG, JIAHUI CHEN, YIYING TONG, GUO-WEI WEI

Abstract. As key subjects in spectral geometry and spectral graph theory respectively, the Hodge Laplacian and the graph Laplacian share similarities in their realization of vector calculus, through the gradient, curl, and divergence, and by revealing the topological dimension and geometric shape of data. These similarities are reflected in the popular usage of “Hodge Laplacians on graphs” in the literature. However, these Laplacians are intrinsically different in their domains of definitions and applicability to specific data formats, hindering any in-depth comparison of the two approaches. To bring the graph Laplacian and Hodge Laplacian on an equal footing for manifolds with boundary, we introduce Boundary-Induced Graph (BIG) Laplacians using tools from Discrete Exterior Calculus (DEC). BIG Laplacians are defined on discrete domains with appropriate boundary conditions to characterize the topology and shape of data. The similarities and differences of the graph Laplacian, BIG Laplacian, and Hodge Laplacian are examined. Through an Eulerian representation of 3D domains as level-set functions on regular grids, we show experimentally the conditions for the convergence of BIG Laplacian eigenvalues to those of the Hodge Laplacian for elementary shapes.

Key words. Hodge Laplacians, spectral graph theory, spectral geometry, algebraic topology, differential geometry

AMS subject classifications. 05C50, 58A14, 20G10

1. Introduction. The Laplacian operator Δ is ubiquitous, proving a useful formalism in many scientific fields, including spectral geometry, differential geometry, spectral graph theory, and algebraic topology. Simply stated, it computes how a function deviates from average values in a local neighborhood. Classically, this operator is used to study problems such as steady state, heat diffusion and wave propagation but has since found many other uses. In particular, with recent advances in machine learning and its connection to the field of Topological Data Analysis (TDA) [29, 9], the eigenvalues of the Laplacian, or spectra, are often used to describe the shape of data and predict related properties [21, 20, 11, 22].

The de Rham-Hodge theory provides both topological and geometric characteristics of manifolds via tools from differential geometry. The relationship between the de Rham-Hodge Laplacian (or Hodge Laplacian) and de Rham-Hodge theory is given by an isomorphism between the operator’s kernel, harmonic forms, and the cohomology classes of manifolds. The dimension of the kernel of the k -Laplacian $k \in \mathbb{Z}$, also known as the Betti number β_k , counts the number of k -dimensional holes. Specifically, β_0 is the number of connected components, β_1 shows the number of tunnels, and β_2 represents the number of cavities. The first nonzero eigenvalue, known as the Fiedler value, or principal eigenvalue, in graph theory describes connectedness. The Hodge Laplacian is a vital tool in spectral geometry. In 1966, Mark Kac [14], once asked if one can determine the shape of a drum from its sound frequencies. More specifically, the question asks if eigenvalues of the Laplacian can uniquely determine geometric properties. While in general it may not be possible to determine the shape of the drum given the spectra due to isospectral manifolds, this question still stimulates various developments in algebraic topology and differential geometry. Recently, speaking to the importance of higher frequency spectral values, in Ref. [18] the connection between the Laplacian spectra and a shape is learned and used to generate an unknown shape from only its Laplacian spectrum. The newly developed evolutionary de Rham-Hodge theory [4] may have a high potential to break the degeneracy of the isometry class of a manifold by generating a family of submanifolds via a filtration.

The field of spectral graph theory also has a rich history distinct from de Rham-Hodge theory [5, 23]. With the wide use of applications of graphs in the 1970s and 1980s, the combinatorial or graph Laplacian [12, 13], a discrete variant of the Hodge Laplacian, gained popularity. The graph Laplacian and its spectrum are proved valuable in the study of molecular stability [10], electrical networks [8], biomolecule analysis [25, 19], neuroscience [15], ranking [26], deep learning [3], and many others. The analogy between the graph Laplacian and Hodge Laplacian was demonstrated in their implementation of vector calculus and description of the topology and shape of data [16]. In these cases, the underlying graph structure of the data is considered and given a clique-based simplicial complex structure and the graph Laplacian resembles the Hodge Laplacian defined on compact manifolds without boundary. Hodge Laplacians on graphs [16] can be regarded as a way to enrich graph theory with versatile tools from differential geometry. However, the graph Laplacian is inherently defined on (discrete) point cloud data, while the Hodge Laplacian is defined on continuous manifolds or volumetric data. Moreover, in many applications, the Hodge Laplacian deals with manifolds with boundary [28], whereas, there is no notion of boundary for the graph Laplacian. For these reasons, the graph Laplacian is conceptually incompatible with the Hodge Laplacian.

To put the graph Laplacian and the Hodge Laplacian on an equal footing for manifolds with boundary, we introduce a new Boundary-Induced Graph (BIG) Laplacian. The BIG Laplacian preserves the discrete nature of graph theory while fully recognizing the graph Laplacian’s capability to perform differential calculus through enforcing appropriate boundary conditions. Specifically, we discuss Dirichlet and Neumann conditions. A regular grid representation of surfaces also ensures that the BIG Laplacian can numerically deliver results similar to those of the Hodge Laplacian as shown by our test cases. We further discuss when the eigenvalues of the clique-based graph Laplacian perform unfavorably as opposed to the BIG Laplacian, which is compared to the Hodge Laplacian. Though all operators discussed may be used interchangeably in the simple case of computing Betti numbers, we point out some key differences when seeking higher frequency spectral information, depending on model representation, and when requiring certain boundary conditions. As an independent formulation, the BIG Laplacian may find its versatile applications without depending on its relation to the Hodge Laplacian.

1.1. Overview. First, in Section 2, we outline the theory for multidimensional Laplacian operators defined using differential forms. Then, Section 2.1 contains a synopsis of the continuous spectral de Rham-Hodge theory with Section 2.2 describing the differential form of the Laplacian on bounded domains. Sections 2.3 and 2.4 cover the representations of discrete surfaces, the discretization of the mentioned theories using Discrete Exterior Calculus (DEC), and the usual graph Laplacians used in this area. After covering the necessary background, we present a novel implementation of the boundary-aware graph Laplacians for 3D volumes to be comparable to the discrete Hodge Laplacian in Section 3. Then through simple examples and in-depth numerical calculations in Sections 4 and 5, we explore the different Laplacians defined through varying model representations, regular grid Eulerian and tetrahedral Lagrangian, as well as differing boundary conditions, Dirichlet and Neumann. To summarize, we

- introduce the BIG Laplacian alongside the Hodge Laplacian for manifolds with boundary,
- illustrate the differences among the usual graph Laplacian, new BIG Laplacian, and the Hodge Laplacian, and

- show the numerical similarities between the BIG Laplacian and Hodge Laplacian.

2. Background. In this section, we briefly review the continuous theory on Hodge k -Laplacians and how they are commonly discretized to Hodge Laplacians defined on simplicial complexes through the use of Hodge stars. Then, we define the (arbitrary-order) graph Laplacians and discuss its relation to the Hodge Laplacians.

2.1. Continuous de Rham-Hodge theory. Most important physical equations expressed in multivariable calculus can be unified using methods from differential forms and exterior calculus. These methods naturally lead to the de Rham-Hodge theory, in which differential geometry, algebraic topology, partial differential equation, and their relationship to spectral graph theory are revealed for analysis. Fundamentally, de Rham-Hodge theory states that the harmonic part of the spectrum of the Laplacian operator can be used for unique presentations of topological structures, more precisely, the cohomology groups of manifolds. Here a brief overview of the necessary components of continuous de Rham-Hodge theory is provided to define the de Rham-Hodge and graph Laplacians and obtain useful information from their spectral analysis.

Given a manifold M , a differential k -form $\omega_k \in \Omega^k(M)$ is a quantity that can be integrated over a k -dimensional domain¹. While the following theory holds for surfaces, or more generally Riemannian manifolds, we will mainly consider volumes in order to introduce the concept of boundary conditions in practical problems and increase the applicability of this study. This means that 0-, 1-, 2-, and 3-forms are considered. In 3D, 0- and 3- forms can be understood as scalar fields, due to their one degree of freedom (DoF) per point, while 1- and 2- forms are understood as vector fields with three DoFs per point. From this point, applying certain combinations of exterior calculus operators, such as the exterior derivative and Hodge star, to differential forms unifies the gradient (∇), divergence ($\nabla \cdot$), curl ($\nabla \times$), and thus the Laplacian ($\Delta, \nabla \cdot \nabla, \nabla^2$) operators in vector field analysis.

In differential geometry, the exterior derivative d , also known as the differential operator, explains how quickly a k -form changes in every $(k+1)$ -dimensional direction. In fact, d acts as the known gradient, curl, and divergence when applied to 0-, 1-, and 2-forms, respectively. Furthermore, $d_k : \Omega^k(M) \rightarrow \Omega^{k+1}(M)$ has the essential property that $d_{k+1} \circ d_k = 0$. Given a manifold, the L_2 inner product on the space of k -forms defines the adjoint operators of d_{k-1} as the codifferential operators $\delta_k : \Omega^k(M) \rightarrow \Omega^{k-1}(M)$. The spaces of differential forms creates a cochain complex or more specifically the de Rham complex,

$$\Omega^0(M) \xrightleftharpoons[\delta_1]{d^0} \Omega^1(M) \xrightleftharpoons[\delta_2]{d_1} \Omega^2(M) \xrightleftharpoons[\delta_3]{d_2} \Omega^3(M).$$

The centerpiece of the de Rham-Hodge theory is the relation between the de Rham complex and the space of harmonic forms or cohomology groups $\mathcal{H}^k = \ker d_k \cap \ker \delta_k$ as

$$\ker d_k = \mathcal{H}^k \oplus \text{im } d_{k-1}.$$

Furthermore,

$$\mathcal{H}^k(M) \cong \mathcal{H}_\Delta^k(M),$$

¹We will try to stick to the notation where the dimension is a subscript except for topological spaces or other special groups, when the dimension will be a superscript. Occasionally the dimension may be left out if clear from the context.

where $\mathcal{H}_\Delta^k(M) = \{\omega | \Delta\omega = 0\}$ is the kernel of the Laplace-de Rham, or de Rham-Hodge Laplacian, operator $\Delta \equiv d\delta + \delta d = (d + \delta)^2$. Through Stokes' theorem, cohomology groups are isomorphic to homology groups, which allow for the categorization of surfaces. Specifically, Betti numbers, $\beta_k = \dim \mathcal{H}^k$, give the count for the number of k -dimensional holes and can be found by calculating the size of the null space of Δ . Fundamentally, these harmonic forms are the 0-frequency spectral bases for differential forms, which allow us to study the structure of M . Instead of defining the Laplace operator with δ , it can be rewritten using the Hodge star operator \star which identifies a k -form with its complementary or dual $(n - k)$ -form for an n -manifold. Precisely, $\delta_k := (-1)^k \star d \star$ (in 3D) so that the scalar Laplacian is $\Delta_0 = \star d \star d$ and the k -Laplacian is

$$(2.1) \quad \Delta_k = (-1)^{k+1} \star d \star d + (-1)^k d \star d \star.$$

Note that the Δ_1 and Δ_2 can be regarded as the vector Laplacian as they act on vector fields.

2.2. Boundary conditions. Before further discussing the differential form version of the Laplacian on domains embedded in 3D Euclidean space, certain boundary conditions must be considered to ensure the operator is well-posed. Two common and useful choices are to have a differential form ω either normal or tangential to the boundary. In the case of normal boundary conditions, also known as (homogeneous) Dirichlet boundary conditions, ω is zero when applied to tangent vectors on the boundary. Using familiar calculus definitions for a scalar function f , the Dirichlet boundary condition is $f|_{\partial M} = 0$. Similarly, for tangential boundary conditions, also called a Neumann boundary condition, $\star\omega$ is zero when applied to tangent vectors on the boundary. Noting that the \star operator identifies primal to dual elements and is like turning line integrals to fluxes. Such a condition on a 1-form represented by a vector field \mathbf{v} can be expressed as $\mathbf{n} \cdot \mathbf{v}|_{\partial M} = 0$, where \mathbf{n} is the boundary normal, i.e., the normal component of \mathbf{v} is 0.

As a consequence, an update to the continuous setting is required when speaking in terms of vector fields. Enforcing that for tangential vector fields, i.e., normal 2-forms or tangential 1-forms, means satisfying one Dirichlet condition $\mathbf{v} \cdot \mathbf{n} = 0$ and two Robin conditions $\mathbf{t}_1 \cdot \nabla_{\mathbf{n}} \mathbf{v} + \kappa_1 \mathbf{t}_1 \cdot \mathbf{v} = 0$, $\mathbf{t}_2 \cdot \nabla_{\mathbf{n}} \mathbf{v} + \kappa_2 \mathbf{t}_2 \cdot \mathbf{v} = 0$, here \mathbf{t}_1 and \mathbf{t}_2 are the two local tangent directions forming an orthonormal coordinate frame with surface normal \mathbf{n} and κ_1 and κ_2 are the sectional curvatures along the coordinate directions. These conditions effectively enforce no contribution from the curl along tangential directions. On the other hand for normal vector fields, i.e., tangential 2-forms or normal 1-forms, this means satisfying two Dirichlet conditions $\mathbf{v} \cdot \mathbf{t}_1 = 0$ and $\mathbf{v} \cdot \mathbf{t}_2 = 0$ and one Robin condition $\mathbf{n} \cdot \nabla_{\mathbf{n}} \mathbf{v} + 2H \mathbf{n} \cdot \mathbf{v} = 0$, where H is mean curvature, to enforce zero contribution from divergence.² Given these extra conditions, our harmonic space is now of finite dimension so that the kernel of the Laplacians is also finite dimensional and agrees with the corresponding absolute/relative homology dimensions.

In terms of differential forms, let Ω_t be the space of tangential forms with tangential differential so that $\omega_t \in \Omega_t$ if and only if $\star\omega_t|_{\partial M} = 0$ and $\star d\omega_t|_{\partial M} = 0$. One may interpret it that ω has $\binom{n}{k}$ DoFs per point, whereas $\star\omega|_{\partial M}$ has $\binom{n-1}{n-k}$ DoFs, so $\star d\omega|_{\partial M}$ provides the additional $\binom{n-1}{n-(k+1)} = \binom{n}{k} - \binom{n-1}{n-k}$ DoFs. In particular, for Neumann boundary condition of a 0-form f , $\star f|_{\partial M} = 0$ is automatic since its an n -form evalu-

²These conditions are consistent with the differential form boundary conditions in Refs.[27, 28, 4]. However, their vector field boundary conditions are correct only for flat boundary surfaces.

ated in an $(n-1)$ -D space, and $\star df|_{\partial M}$ provides the familiar $\mathbf{n} \cdot \nabla f|_{\partial M} = 0$. Similarly, let Ω_n be the space of normal forms with normal codifferential so that $\omega_n \in \Omega_n$ if and only if $\omega_n|_{\partial M} = 0$ and $\delta\omega_n|_{\partial M} = 0$.

Enforcing such modified boundary conditions means to restrict Δ to Ω_t or Ω_n . The restricted harmonic forms are $\mathcal{H}_n^k = \mathcal{H}^k \cap \Omega_n$ and $\mathcal{H}_t^k = \mathcal{H}^k \cap \Omega_t$ which are associated with the kernels of $\Delta_{k,n}$ and $\Delta_{k,t}$ respectively. Due to the dimensionality of $k = \{0, 1, 2, 3\}$ and since we are considering two types of boundary conditions, normal and tangential, there are eight Laplacian operators denoted $\Delta_{k,n}$ and $\Delta_{k,t}$. However, using the duality between k and $(n-k)$ -forms, the space of normal k -forms can be identified with the space of tangential $(n-k)$ -forms. This reduces the eight spectra to four distinct spectra, which may be further reduced to three using Hodge decomposition [28].

2.3. Discrete de Rham-Hodge theory. To discretize de Rham-Hodge theory, first the input domain must be specified. It is common to collect sample points of the input shape as a point cloud, where each point is presented by its 3D coordinates. The connectivity of points may be given through mesh connectivity (cell complex structure) or prescribed by any number of criteria. A Delaunay triangulation [6] for a given set of vertices is defined by its dual structure, the corresponding Voronoi diagram [24]. A Voronoi dual cell of a vertex v is the set of points P around v such that the distance between any $p \in P$ is less than the distance between p and any other vertex,

$$V_i = \{v \in \mathbb{R}^q \mid \|v - p_i\| \leq \|v - p_j\|, \quad \forall p_j \in P\}.$$

The Voronoi diagram is the set of Voronoi cells, which is defined as

$$\text{Vor}P = \{V_i \mid \forall i \in \{1, 2, \dots, |P|\}\},$$

where $|P|$ is the number of points in set P . The primal 2D (3D, respectively) Delaunay triangulation can also be defined by the empty circle (sphere) property, that the circumscribing circle (sphere) of a face (cell) does not contain any vertex in its interior (cell). This triangulation is unique as long as any four vertices are not co-circular (or any five vertices are not co-spherical).

A Delaunay triangulation is an example of a simplicial complex. A simplicial complex consists of simplices with some additional properties. Generally, a k -simplex σ_k is the convex hull of $k+1$ affinely independent points in \mathbb{R}^n . In this way, a k -simplex is discretely defined as an ordered set of $k+1$ vertices, $\sigma = [v_0, v_1, \dots, v_k]$ where its incident $(k-1)$ -simplices form a type of boundary of σ . Furthermore, k -simplices, for our purposes $k \in \{0, 1, 2, 3\}$, correspond to their k -dimensional elements: vertices, edges, faces, and cells. It is useful to use the terms faces and cofaces when referring to relations between simplices. A k -simplex can be referred to as a k -face of a simplex τ , if σ is in the boundary of τ , i.e., it is a simplex formed from a subset of the vertices of τ . In this case, τ is a coface of σ . A simplicial complex K consists of simplices under the following conditions:

1. If $\sigma_j \in K$ and σ_k is a face of σ_j , then $\sigma_k \in K$.
2. The non-empty intersection of any two simplices $\sigma_j, \sigma_k \in K$ is a face of σ_j and σ_k .

Given a point cloud, different simplicial complexes can be defined with simple criteria such as the alpha complex, Čech complex, and Vietoris-Rips complex. Given a set of vertices $V = \{v_0, v_1, \dots, v_{N_0-1}\}$, embedded in \mathbb{R}^3 , consider a nested family

of simplicial complexes. This family, called a filtration, is created for a positive real/integer number α , the filtration parameter. Specifically, using the alpha complex filtration as an example, the filtration of subcomplexes $(K_\alpha)_{\alpha=0}^m$ is

$$\emptyset = K_0 \subseteq K_1 \subseteq K_2 \subseteq \cdots \subseteq K_m = K.$$

which gives the final simplicial complex K , the Delaunay triangulation. Each subcomplex can be considered as an α -complex, the collection of Delaunay simplices whose smallest empty circumsphere has a radius $\leq \alpha$. Such simplicial complexes are computed in the field of TDA in the context of persistence of features over time where the Laplacian is computed for varying filtration parameter values.

If starting from the perspective of graphs, where $G = (V, E)$ is an undirected graph generated from a point cloud, a simplicial complex can be realized from cliques as in Ref. [16]. A k -clique $K_k(G)$ is the set of vertices v_j, v_k such that the edge connecting those vertices $e_{jk} := \{v_j, v_k\} \in E$. For example, triangles or 2-simplices are 3-cliques. In this way, a simplicial complex can be defined using subsets of V as discussed but by specifying cliques and is called the clique complex of G . The clique complex can be seen as a special case of Vietoris-Rips complex. Given such an input, the discrete treatment of de Rham-Hodge theory, which preserves many properties of its continuous counterpart, can be described using the language of differential forms as acted on by boundary and Hodge star operators by Discrete Exterior Calculus (DEC [7]). For an equivalent finite element approach, see Ref. [1].

The boundary operator ∂ of a k -simplex is a $(k-1)$ -chain (i.e., a formal linear combination of $(k-1)$ -simplices)

$$(2.2) \quad \partial\sigma = \sum_{i=0}^k (-1)^i [v_0, v_1, \dots, \hat{v}_i, \dots, v_k],$$

where \hat{v}_i is the vertex omitted. It can be linearly extended to a linear operator on k -chains. In the matrix form, the k -boundary operator B_k has the number of $(k-1)$ -simplices rows and the number of k -simplices columns. In the matrix, an (i, j) entry is $+1$ or -1 if the i -th $(k-1)$ -simplex is on the boundary of the j -th k -simplex and 0 if it is not on the boundary. The sign is determined by the orientation of the $(k-1)$ -simplex relative to the orientation of the k -simplex. The orientations can be arbitrarily chosen for the simplices forming a basis for the space of chains. Next, since the boundary operator ∂ is the adjoint of the exterior derivative d , it is also called the coboundary operator. One can take the transpose of the proposed B_k to get D_{k-1} , the discrete representation of d when k -forms ω are discretized to k -cochains w , the dual of k -chains, by $w_\sigma = \int_\sigma \omega$. This equivalence to the boundary operator can also be seen through Stokes' theorem,

$$\int_{\partial\sigma} \omega = \int_\sigma d\omega,$$

which means that calculating $d\omega$ on a simplex σ can be replaced with a calculation of ω on the boundary of σ . Now $D_k = B_{k+1}^T$ is the signed incidence matrix between k and $(k+1)$ -simplices.

To discretize the Hodge star \star , the concept of duality between Delaunay triangulation and Voronoi diagram is further explored. Since the Hodge star maps k -forms to $(n-k)$ -forms, we need a way to transform primal k -simplices to dual $(n-k)$ -cells and vice versa. One simple way to calculate the Hodge star, is to discretize $\star\omega$ by its

integral on Voronoi dual cells when ω is represented by the integral on the Delaunay simplices. In this case, we call ω as a primal form and $\star\omega$ a dual form. The Hodge star can then be discretized as a diagonal matrix S_k as the ratio between the length, area, or volume of a dual $(n - k)$ -Voronoi-cell and its primal k -simplex. For this reason, the Hodge star is essentially a scaling factor and can be highly dependent on the tessellation. Other more accurate Hodge stars can be computed, such as the Galerkin Hodge star [2] through higher-order basis functions.

Next, the discrete Hodge Laplacian follows from 2.1,

$$(2.3) \quad L_k^H = D_k^T S_{k+1} D_k + S_k D_{k-1} S_{k-1}^{-1} D_{k-1}^T S_k,$$

which is a symmetric matrix where $S_k^{-1} L_k^H$ is the discrete counterpart of Δ_k . The signs in the above equation are consistent with the proper use of D_k^T to discrete $(-1)^k d_{n-k-1}$. As discussed, to discover geometrical information, it helps to investigate not only the null space of the Laplacian but the entire spectra, the eigenvalues of the Laplacian. While the size of the null space of the k th-Laplacian, the k th-Betti number, reveals the number of k -dimensional holes (β_0 is the number of connected components, β_1 is the number of tunnels, β_2 is the number of voids, and $\beta_3 = 0$ as there is no 4-dimensional holes in 3D domains in \mathbb{R}^3), we would also like to investigate non-zero eigenvalues which offer some qualitative information of the shape, especially in the context of machine learning. In fact, the Fiedler value, i.e., the first non-zero eigenvalue, can describe connectivity. Furthermore, the multiplicity of eigenvalues may reveal certain symmetries of a shape.

2.4. The graph Laplacian. The graph Laplacian is defined in a similar way to the Hodge Laplacian as

$$L_k^G = D_k^T D_k + D_{k-1} D_{k-1}^T.$$

For L_0^G , this is precisely the Laplacian used in spectral graph theory [16]. Here Betti numbers correspond to the dimension of nontrivial k -dimensional cycles (i.e., boundaryless k -chains that are not boundaries of $(k + 1)$ -chains). Simply stated, the graph Laplacian disregards the geometric measurements of simplices as encoded by the Hodge star, that being edge length, face area, or cell volume. As discussed in Ref. [16], the graph Laplacian only requires the adjacency information contained in boundary operators. Furthermore, the discrete operators proposed are sparse and positive semi-definite, which allows for the use of efficient solvers. While the 0-Laplacian can incorporate edge weights to have a weighted graph Laplacian, there is no generic way to assign proper weights to higher-order simplices other than the actual Hodge star calculation, which are almost never a scaled identity matrix.

For a clique complex, the resulting k -Laplacian is almost never that of the (graph) Laplacian of a simplicial mesh. Čech complexes also do not share the same D_k with a simplicial mesh. While, the alpha complex does provide incidence matrices similar to a manifold mesh aside from some degeneracy, the resulting Laplacians without S_k still produces spectra that are far from those of Hodge Laplacians. Recall from graph theory that the degree of a vertex v is the number of adjacent vertices, denoted $\deg(v)$. With the clique complex, the adjacency information between vertices extends induces incidence, i.e., the face/coface relationship between k and $(k + 1)$ -simplices. For example, given the end point vertex v of an edge e , v is incident to e .

Wang et al. [25] discussed the general case when the simplicial complex is not necessarily induced from the clique in the graph. It is useful to introduce the notion of adjacency, incidence, and degree for all simplices in the complex. Two simplices

σ^i and σ^j are called upper adjacent, denoted $\sigma_k^i \overset{U}{\sim} \sigma_k^j$, if they are incident to the same $(k+1)$ -simplex. The upper degree $\deg_U(\sigma_k)$, is the number of $(k+1)$ -simplices that are faces of σ_k . Similarly, two k -simplices are called lower adjacent if they are adjacent, or share the same $(k-1)$ -simplex. The lower degree $\deg_L(\sigma_k)$, is the number of $(k-1)$ -simplices that are cofaces of σ_k . Then the degree of a k -simplex, $k > 0$ is,

$$\deg(\sigma_k) = \deg_U(\sigma_k) + \deg_L(\sigma_k).$$

To explicitly define the graph Laplacian, an orientation for the simplicial complex must be specified. While the orientation itself is arbitrary, each simplex, except for vertices, is given a direction. For simplex σ_k , its ordering is defined by an ordering on its vertex set, $\sigma_k = [v_0, \dots, v_k]$. The entries of the graph Laplacian matrix are then explicitly defined as follows³,

$$(L_0^G)_{ij} = \begin{cases} \deg(\sigma_0^i) & \text{if } i = j. \\ -1 & \text{if } \sigma_0^i \overset{U}{\sim} \sigma_0^j. \\ 0 & \text{otherwise,} \end{cases}$$

and for $k > 0$

$$(L_k^G)_{ij} = \begin{cases} \deg(\sigma_k^i) & \text{if } i = j. \\ 1 & \text{if } i \neq j, \sigma_k^i \overset{U}{\sim} \sigma_k^j \text{ and } \sigma_k^i \overset{L}{\sim} \sigma_k^j \text{ with the same orientation.} \\ -1 & \text{if } i \neq j, \sigma_k^i \overset{U}{\sim} \sigma_k^j \text{ and } \sigma_k^i \overset{L}{\sim} \sigma_k^j \text{ with different orientation.} \\ 0 & \text{if } i \neq j \text{ and either } \sigma_k^i \overset{U}{\sim} \sigma_k^j \text{ or } \sigma_k^i \overset{L}{\not\sim} \sigma_k^j. \end{cases}$$

3. The Boundary-Induced Graph (BIG) Laplacian. The clique-based graph Laplacian, while useful for calculating Betti numbers, differs drastically from the Hodge Laplacian given its current form. This is due to the fact that the graph Laplacian is fully determined by graph connectivity and lacks geometry awareness. Only if data points are uniformly distributed with regular graph edges can the spectra be comparable given perhaps some scaling factors. However, such a distribution is only possible on a 2D plane given explicit graph and clique complex representations. Furthermore, real-world applications require some notion of behavior on the boundary, not previously explored in the context of the graph Laplacian. To bridge these gaps, we propose a 3D boundary-induced graph Laplacian defined implicitly on a regular Cartesian grid.

3.1. Eulerian representation. From the context of fluid simulation, the distinction between explicit and implicit methods can be described by Lagrangian and Eulerian discretizations. The Lagrangian method describes the motion of particles using a tetrahedral mesh and chooses the reference point of particles, while the Eulerian representation describes the motion of particles embedded in an enlarged domain. As commonly used in level set-based methods, we employ an Eulerian method using a Signed Distance Function (SDF) to the boundary surface of a volume M on a regular grid as opposed to Lagrangian methods. This allows the underlying connectivity of points to have a rigid and uniform structure in order for the spectra of BIG Laplacians to resemble those of the Hodge Laplacians and thus the actual Laplacians on the original smooth surface or surface bounded volume.

³We follow the notations in Ref. [25], except for their typo in the diagonal entry.

In addition to facilitating the proper comparison of the different Laplacians, a regular grid also helps to simplify the data structures used. Since grid elements have a fixed length, area, and volume, the effect of the Hodge star, or lack thereof in the case of the BIG Laplacian, is minimized. The grid spacing or grid length is given as input and though not proven in this work, a reduction in grid length is empirically shown to increase the accuracy of our method as demonstrated in Section 5. Similar to the simplicial complex differential operator, our D_k includes grid elements forming a cell complex instead of a simplicial complex.

3.2. Boundary condition correction. As already included in the study of the usual discrete Hodge Laplacian, boundary conditions are now introduced for the BIG Laplacian. By simply checking the sign of SDF values of grid points, we can tell which cells are on the boundary of M and thus enforce particular boundary conditions through updates to D_k . As discussed, two types of boundary conditions are considered, normal (Dirichlet) and tangential (Neumann). In the discrete Lagrangian setting (simplicial complexes, i.e., triangle/tetrahedron meshes in 2D/3D), these conditions correspond to exclusion, in the normal case, or inclusion, in the tangential case, of boundary elements. The exclusion is done directly in D_k operators as rows and columns on the boundary are kept or removed. Accordingly, we denote the differential operator for normal forms as $D_{k,n}$ and the for tangential forms as $D_{k,t}$.

In our Eulerian setting, the cells are not aligned with the boundary as we do not have an explicit boundary surface to enable the exclusion of the surface to the volume. Fortunately, on regular grids, both boundary conditions can be implemented based on the cells of either the primal or dual grid. For normal boundary conditions, we include all cells that are either inside or intersect with the boundary, i.e., at least one of its vertices is inside. For tangential boundary conditions, we include all cells whose corresponding dual cells are inside or partially inside. In fact, since the dual grid structure is also a Cartesian grid staggered with the primal grid (by a displacement of $\frac{1}{2}(l_g, l_g, l_g)$) we only need to implement one of the boundary conditions $L_{k,n}$ as the other $L_{n-k,t}$ would be strictly equivalent to a slightly shifted SDF input (or equivalently, a slightly shifted grid).

Then, to facilitate the matrix conversions, a projection or selection matrix P_k may be used. P_k zeros out any columns or rows corresponding to k and $k+1$ grid elements to be removed as either exterior to the model or as prescribed by the boundary condition. Then the new exterior matrices are

$$D_{k,n} = P_{k+1} D_k P_k^T,$$

and the normal BIG Laplacians are

$$(3.1) \quad L_{0,n}^B = D_{0,n}^T D_{0,n}$$

$$(3.2) \quad L_{1,n}^B = D_{1,n}^T D_{1,n} + D_{0,n} D_{0,n}^T$$

$$(3.3) \quad L_{2,n}^B = D_{2,n}^T D_{2,n} + D_{1,n} D_{1,n}^T$$

$$(3.4) \quad L_{3,n}^B = D_{2,n} D_{2,n}^T.$$

To solve for the spectra, we use a scaling diagonal matrix, so that the results of the BIG Laplacian are comparable to the Hodge Laplacian as calculated in the next section. In particular, let S_k^B have $1/l_g^2$ on the diagonal with correct size for the number of k grid elements. Then with projection matrices, $P_k(S_k^B)^{-1} P_k^T L_k$ corresponds to Δ_k .

3.3. Hodge Laplacian on regular grids. Now the BIG Laplacian can be directly compared to the usual Hodge Laplacian, though we include some updates to the Hodge Laplacian on the regular grid for completeness. For simplicity and numerical reasons, the k -Hodge star is usually implemented as a diagonal matrix S_k with entries as the ratio between the $(n - k)$ -volume of the Voronoi (or other dual structure) $(n - k)$ -cell and the k -volumes of the primal k -simplex and is highly dependent on the tessellation. More accurate Hodge stars can be discussed but are left for future work on numerical accuracy. Yet, given our regular grid representation, Hodge stars are simple and uniform to calculate for grid elements located completely in the interior of the model. With grid edge length l_g , values of S_0 are l_g^3 , S_1 are l_g^2/l_g , S_2 are l_g/l_g^2 , and S_3 are $1/l_g^3$. However, we modify the Hodge star slightly for edges, faces, and cells that cross the boundary surface following [17] with extensions to all orders for both boundary conditions, since they only implemented normal 1-forms representing vorticity fields of tangential velocity fields.

As with D_k , boundary conditions should also be considered for S_k . In particular, For $S_{k,n}$, the primal cell volumes are modified with dual cell volume unaltered, whereas for $S_{k,t}$, dual cell volumes are modified with the primal cell volume unaltered. For instance, in the case of 2-forms ω with normal boundary conditions, in order to define $S_{1,n}$, $S_{2,n}$, and $S_{3,n}$, we require that ω is zero when applied to tangent vectors on the boundary. This is equivalent to saying that surface patches in the Lagrangian sense offer no contribution on the boundary or that the flux through the boundary is zero. As before with $D_{k,n}$ we use the projection matrices P_k as follows,

$$S_{k,n} = P_k S_k P_k^T.$$

For example, we alter S_2 so that grid faces which cross the boundary only contribute as much as the portion of the face which resides inside of the model. For the normal boundary condition, the dual cell sizes are not altered [17]. Thus, the Hodge star S_2 acts as a scaling factor, a ratio of original dual edge length to the portion of primal face area inside of the model \mathcal{A}_i . Given that the grid spacing is l_g ,

$$S_{2,n}(i, i) = \frac{l_g}{\mathcal{A}_i}$$

For face f_i on the interior or crossing the boundary of M . Note that for faces f_j completely inside of the model, $S_{2,n}(j, j) = 1/l_g$. The situation is similar for $S_{1,n}$ and $S_{3,n}$ in that the primal length or volume inside the model is considered. Approximations of the inside portions are computed using the SDF values, the convex hull of inside simplices, and the marching cubes algorithms. Here, S_0 is unchanged since a vertex is dimensionless, so it is either inside or outside. For the numerical implementation, we avoid division by near zero primal cell volumes. Any primal k -cell with a volume below a preset positive threshold ($\epsilon \ll l_g$) will have its volume rounded up to ϵ^k . This prevents the large scaling factors that can potentially distort the results, while maintaining the correct Laplacian kernel dimensions.

The normal Hodge Laplacian uses the D_k operators as in the BIG Laplacian but with S_k operators for scale and are

$$(3.5) \quad L_{0,n}^H = D_{0,n}^T S_{1,n} D_{0,n}$$

$$(3.6) \quad L_{1,n}^H = D_{1,n}^T S_{2,n} D_{1,n} + S_{1,n} D_{0,n} S_{0,n}^{-1} D_{0,n}^T S_{1,n}$$

$$(3.7) \quad L_{2,n}^H = D_{2,n}^T S_{3,n} D_{2,n} + S_{2,n} D_{1,n} S_{1,n}^{-1} D_{1,n}^T S_{2,n}$$

$$(3.8) \quad L_{3,n}^H = S_{3,n} D_{2,n} S_{2,n}^{-1} D_{2,n}^T S_{3,n}.$$

All matrices are symmetric and positive semi-definite where $(S_{k,n})^{-1}L_{k,n}^H$ corresponds to Δ_k . We solve for the eigenvalues and eigenbasis functions through a generalized eigenvalue problem,

$$L_{k,n}^H \omega_k = \lambda_k S_{k,n} \omega_k.$$

See algorithm 3.1 for more details.

Algorithm 3.1 Assemble coboundary, Hodge star, and projection matrices.

Input: dimension $k \in \{1, 2, 3\}$
 primal k -areas $\mathcal{A}_k^{\text{primal}}(i)$ for $i \in \{0, 1, \dots, |\Sigma_k| - 1\}$
 error tolerance $\epsilon \ll l_g$ {prevents division by 0}

Output: D_{k-1} , S_k , and P_k

- 1: $n \leftarrow 0$
- 2: $P_k, S_k \leftarrow$ empty sparse $|\Sigma_k| \times |\Sigma_k|$ matrix { Σ_k : set of oriented k -cells}
- 3: $D_{k-1} \leftarrow$ empty sparse $|\Sigma_k| \times |\Sigma_{k-1}|$ matrix
- 4: **for** $\sigma_i \in \Sigma_k$ **do**
- 5: **if** any incident gridpoint of $\mathcal{A}_{k,i}^{\text{primal}}$ is inside **then**
- 6: $S_k(i, i) \leftarrow \mathcal{A}_{3-k}^{\text{dual}} / \max(\mathcal{A}_k^{\text{primal}}(i), \epsilon^k)$ {dual $(3-k)$ -area $\mathcal{A}_{3-k}^{\text{dual}} = l_g^{3-k}$ }
- 7: $P_k(n, i) = 1$
- 8: $n \leftarrow n + 1$
- 9: **end if**
- 10: **for** $\xi_j \in \Sigma_{k-1}$ a coface of σ_i **do**
- 11: $D_k(i, j) = 1$ or -1 {depending on orientation}
- 12: **end for**
- 13: **end for**

3.4. The reduced spectrum N, T , and C . Since the space of normal k -forms can be identified with the space of tangential $(n - k)$ -forms the four independent operators in 3.5 are sufficient to represent all eight Laplacians. Furthermore, as the Laplacians are constructed based on the three exterior derivatives, the spectra of these can be decomposed into three distinct parts [27]:

1. T, singular values of the gradient of tangential scalar fields (or equivalently, divergence of tangential gradient fields),
2. N, singular values of the gradient of normal scalar fields (or equivalently, divergence of normal gradient fields),
3. C, singular values of the curl of tangential curl fields (or equivalently, curl of normal curl fields),

The spectrum of each Laplacian can be represented as a combination of one or two of the three singular spectra, potentially adding a zero with a multiplicity based on the corresponding Betti number. This can be illustrated by the fact that variations of $D_k D_k^T$ and $D_k^T D_k$ both show up in L_k and L_{k+1} and each has the same set of nonzero eigenvalues. For example, the spectrum of $L_{0,n}$ appears as part of the spectrum of $L_{1,n}$ from the gradient fields.

4. Differences among Laplacians. To illustrate the differences among the usual graph Laplacian, BIG Laplacian, and Hodge Laplacian, we introduce some simple examples discussing different boundary conditions and spatial discretizations. We start by calculating the Eulerian BIG and Hodge 0-Laplacians and their spectra for 2D shapes over coarse grids, as well as an example for a triangulated (Lagrangian) shape. Next, we show the drastic differences between the Lagrangian clique-based

BIG and Hodge Laplacians in the case of an irregularly sampled ball. We conclude with a figure describing the importance of different boundary conditions and the effect it has on the spectra of Laplacians.

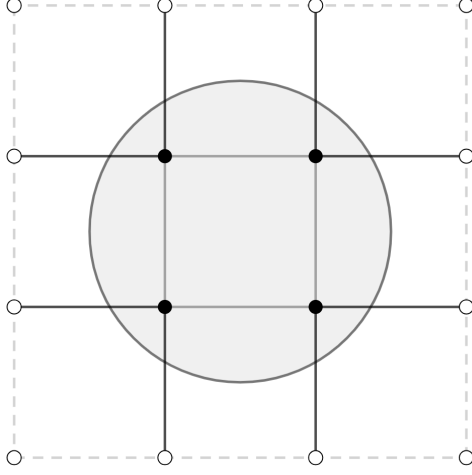


FIG. 1. A unit disk embedded in a 3×3 2D grid with unit grid length.

4.1. 2D calculation with normal boundary condition. In Figure 1, we first present the necessary matrices to compute $L_{0,n}$ for two simple examples, a disk and a square on a 3×3 grid with grid length $l_g = 1$. The disk example illustrates the effect of the Hodge star on the Hodge Laplacian. The 8 edges which cross the boundary of the model (in black in the figure) contribute only their primal edge length, a fraction of the grid edge length to the calculation. In particular, $S_{1,n}$ is the ratio of the dual edge length to the (partial) primal edge length.

Given the unit disk with an embedding as in Figure 1, to compute the 0-Laplacian with normal boundary conditions we first remove the outside edges and vertices, the dashed gray edges and empty circle vertices in Figure 1. The remaining edges are then split into two sets, the solid gray edges inside E_i and the black edges which cross the boundary E_b . Then the coboundary operator is

$$(4.1) \quad D_{0,n} = \begin{bmatrix} -1 & 1 & 0 & 0 \\ 0 & -1 & 1 & 0 \\ 0 & 0 & -1 & 1 \\ 1 & 0 & 0 & -1 \\ -1 & 0 & 0 & 0 \\ 0 & 1 & 0 & 0 \\ 0 & -1 & 0 & 0 \\ 0 & 0 & 1 & 0 \\ 0 & 0 & -1 & 0 \\ 0 & 0 & 0 & 1 \\ 0 & 0 & 0 & -1 \\ 1 & 0 & 0 & 0 \end{bmatrix}$$

noting that the first four edge rows are for those in E_i and have both -1 and 1 entries for their vertex boundaries while the rest of the edges in E_b only have one vertex

included. Denote the primal edge length of edge e_i as $l_p(i)$ then compute the diagonal Hodge star,

$$S_{1,n}(i, j) = 1/l_p(i) \delta_{ij},$$

where δ_{ij} is the Kronecker delta. Note that edges which cross the boundary have primal inside edge length $l_p = 0.37$.

Next we compute the Laplacians,

$$L_{0,n}^H = D_{0,n}^T S_{1,n} D_{0,n} = \begin{bmatrix} 7.41 & -1 & 0 & -1 \\ -1 & 7.41 & -1 & 0 \\ 0 & -1 & 7.41 & -1 \\ -1 & 0 & -1 & 7.41 \end{bmatrix},$$

$$L_{0,n}^B = D_{0,n}^T D_{0,n} = \begin{bmatrix} 4 & -1 & 0 & -1 \\ -1 & 4 & -1 & 0 \\ 0 & -1 & 4 & -1 \\ -1 & 0 & -1 & 4 \end{bmatrix}.$$

The eigenvalues of these matrices are then

$$\lambda_{0,n}^H = \{5.41, 7.41, 7.41, 9.41\} \text{ and } \lambda_{0,n}^B = \{2, 4, 4, 6\}.$$

While the exact eigenvalues for the Hodge Laplacian, as computed from the roots of the Bessel functions squared are

$$\lambda_{\text{exact}} = \{5.7832, 14.682, 14.682, 26.3746\}.$$

Thus, the Hodge Laplacian's principal eigenvalue is much closer than the BIG Laplacian to the expected eigenvalue even for a very coarse sampling of points thanks to the Hodge star. In fact, the clique-based graph Laplacian produces an even more erroneous principal eigenvalue 0, since it can only handle the tangential boundary condition as discussed in Section 4.2.

For a 3×3 square, D_0 remains the same and S_1 is the 12×12 identity matrix since all 12 edges are entirely inside of the model. For this reason, we have

$$L_{0,n}^H = L_{0,n}^B = \begin{bmatrix} 4 & -1 & 0 & -1 \\ -1 & 4 & -1 & 0 \\ 0 & -1 & 4 & -1 \\ -1 & 0 & -1 & 4 \end{bmatrix},$$

$$\lambda_{0,n}^H = \lambda_{0,n}^B = \{2, 4, 4, 6\}, \text{ and for the Hodge Laplacian,}$$

$$\lambda_{\text{exact}} = \{2.1932, 5.4831, 5.4831, 8.773\}.$$

In this case, since the square's boundary is exactly the boundary of the grid domain, the Hodge star is the identity matrix. Thus, the Hodge and BIG Laplacians are identical. However, the eigenvalues in this case still perform favorably even for such a coarse tessellation. The accuracy of eigenvalues improves considerably with a finer resolution as shown in Figure 4 and approaches the exact solution numerically as the resolution increases or the grid length decreases.

4.2. 2D calculation with tangential boundary condition. To illustrate the tangential boundary condition, we consider a 2×2 square in the center of the 3×3 grid in Figure 1. The four solid grid points are the only ones with dual cells that are partially inside the domain. For this particular size, the Hodge stars $S_{0,t}$ and $S_{1,t}$ are both identical matrices, since all the dual cells/edges involved are fully inside the domain. With the following coboundary matrix,

$$(4.2) \quad D_{0,t} = \begin{bmatrix} -1 & 1 & 0 & 0 \\ 0 & -1 & 1 & 0 \\ 0 & 0 & -1 & 1 \\ 1 & 0 & 0 & -1 \end{bmatrix},$$

the Hodge Laplacian is identical to the BIG Laplacian,

$$L_{0,t}^H = L_{0,t}^B = \begin{bmatrix} 2 & -1 & 0 & -1 \\ -1 & 2 & -1 & 0 \\ 0 & -1 & 2 & -1 \\ -1 & 0 & -1 & 2 \end{bmatrix}.$$

Thus,

$$\lambda_{0,t}^H = \lambda_{0,t}^B = \{0, 2, 2, 4\}.$$

Note that the exact spectrum below for the Hodge Laplacian contains 0 with the multiplicity of $\beta_0 = 1$,

$$\lambda_{\text{exact}} = \{0, 2.4674, 2.4674, 4.9348\}.$$

When a 1×1 square is given, the BIG Laplacian remains the same as it ignores the change in the Hodge star. The four dual cell size estimate is changed to $0.5^2/2$ where as the dual edge size estimate is scaled to 0.5, leading to a doubled frequency. While both spectra are far from the exact spectra, the Hodge star-based calculation is much closer even for such an extremely coarse resolution. It is a simple exercise to see that the discrete $L_{0,t}$ has the exact same spectrum as the discrete $L_{2,n}$ on the dual grid.

If a diagonal edge is added, so to triangulate the square as in the Lagrangian method, we add a row to the matrix from 4.2,

$$(4.3) \quad D_{0,t} = \begin{bmatrix} -1 & 1 & 0 & 0 \\ 0 & -1 & 1 & 0 \\ 0 & 0 & -1 & 1 \\ 1 & 0 & 0 & -1 \\ -1 & 0 & 1 & 0 \end{bmatrix}.$$

For the diagonal Hodge star, we use cotangent weights of edges. For the new edge, $S_{1,t}$ is $2 \cot(\pi/2) = 0$ and all other edges are $\cot(\pi/4) = 1$. While $L_{0,t}^H$ remains the same as above, now

$$L_{0,t}^B = \begin{bmatrix} 3 & -1 & -1 & -1 \\ -1 & 2 & -1 & 0 \\ -1 & -1 & 3 & -1 \\ -1 & 0 & -1 & 2 \end{bmatrix}.$$

Whose third eigenvalue is now considerably skewed,

$$\lambda_{0,t}^B = \{0, 2, 4, 4\},$$

while the eigenvalues of $L_{0,t}^H$ remain somewhat close to the expected.

4.3. Impact of Hodge star on clique-based graph Laplacian. Next, we demonstrate the impact of the Hodge star on Lagrangian meshes with irregular sampling. When the true Hodge star operator is not a rescaled identity, even for the interior DoF, and not just for the boundary, the graph Laplacian would be nowhere near the expected spectra, as shown in Figure 2. Whereas, the Hodge star compensates for the irregularity, at least for the first 10 or so eigenvalues.

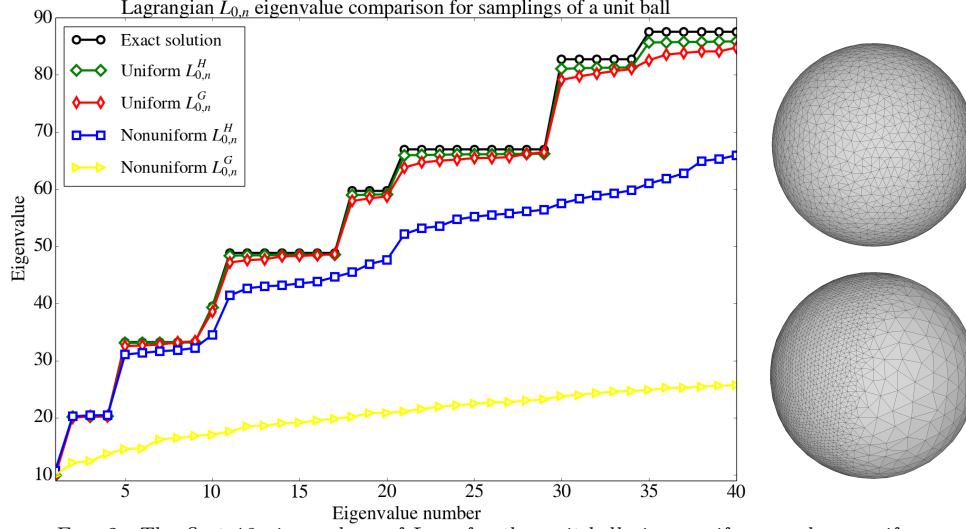


FIG. 2. The first 40 eigenvalues of $L_{0,n}$ for the unit ball given uniform and nonuniform samplings. The Lagrangian graph and Hodge Laplacians are shown (left) for boundary surface average edge length approximately 0.07 (top right) and 0.04 (bottom right).

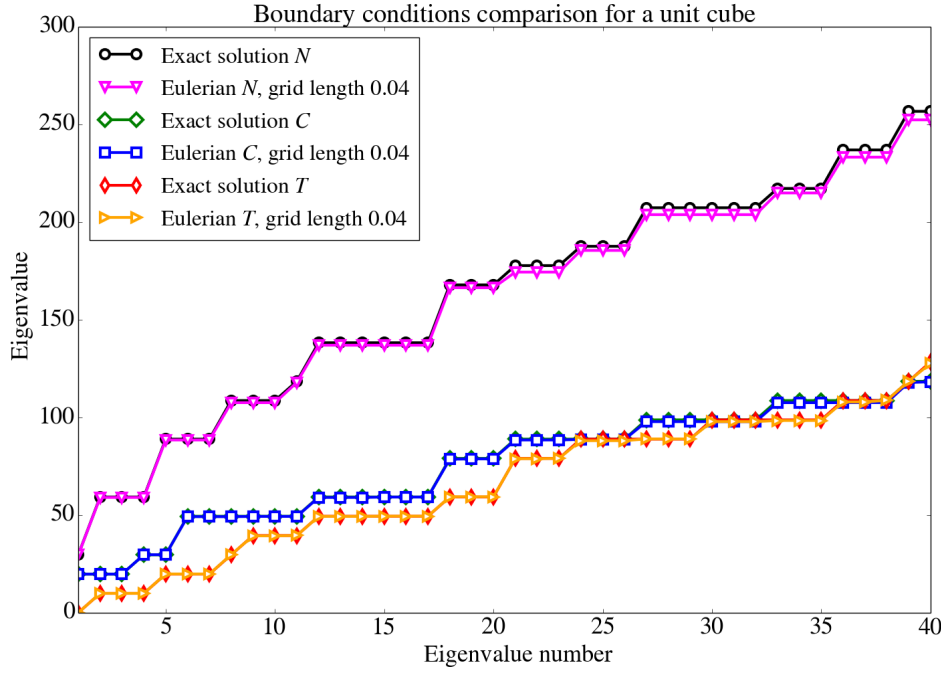


FIG. 3. The first 40 eigenvalues of the three spectral sets N , T , and C for the unit cube. Both exact solutions and Eulerian Hodge Laplacian solutions for grid length 0.04 are shown.

4.4. Justification for boundary conditions. Another test where the clique-based graph Laplacian would also fail is the boundary treatment. If the boundary treatment is not correctly handled for the scalar field Laplacian, the variation between N and T can be large as shown in Figure 3. For the vector Laplacian, the spectra can be either $C \cup N$ or $C \cup T$ depending on the boundary condition, which again are distinct.

5. Similarities among Laplacians. Here we demonstrate the similarities of the Eulerian BIG and Hodge Laplacians as well as to that of the Lagrangian representation of the Hodge Laplacian from [28] by comparing their first 40 eigenvalues for $L_{0,n}$, $L_{1,n}$, and $L_{3,n}$. We also include the exact eigenvalues in the sense of the Hodge Laplacian when available and as outlined in the supplementary material.

5.1. Planar Result. In this 2D example, we computed the 0-Laplacians under normal boundary conditions, i.e., scalar Laplacians with Dirichlet boundary conditions. Figure 4 shows the first 40 eigenvalues for grid edge lengths 0.05 and 0.1 for BIG and Hodge Eulerian Laplacians alongside the solutions to the exact eigenvalue problems. The results for the disk in Figure 4 show how the addition of the Hodge star, in the case of the Hodge Laplacian, improves the results when compared to the exact solution. In fact, the Hodge Laplacian with a twice as large grid length performs nearly as good as the BIG Laplacian. The exact solutions for the disk are found using Bessel functions. Each eigenvalue $\lambda_{n,k}$ is given by the k -th zero of the n -th Bessel function and then they are sorted.

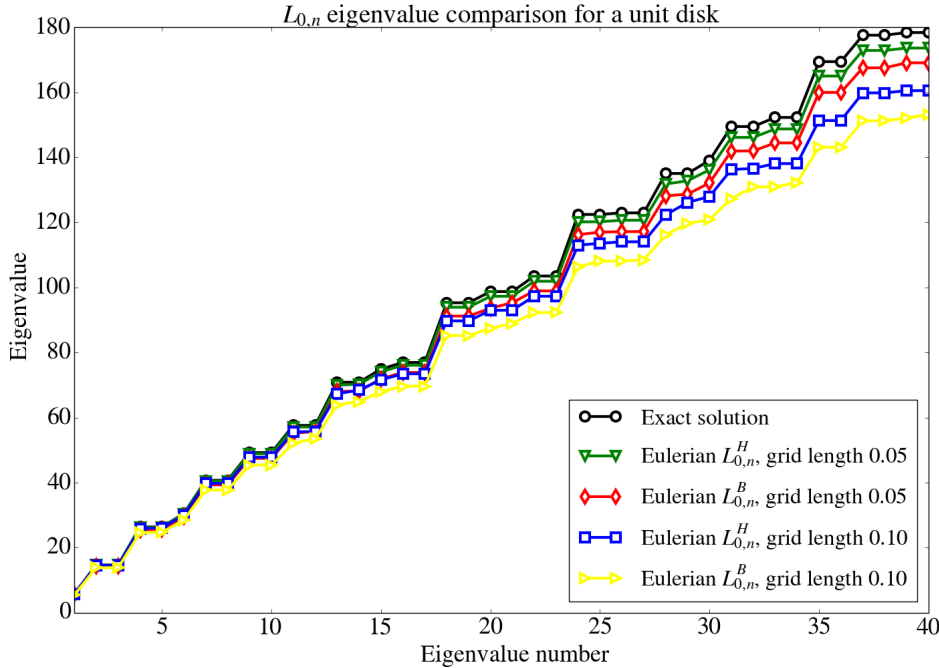


FIG. 4. The first 40 eigenvalues of $L_{0,n}$ for the unit disk. The Eulerian BIG and Hodge Laplacians are shown for two different grid lengths, 0.05 and 0.1.

5.2. Similarities in 3D. Given the duality, in these tests, we compute the 0-, 1-, and 3-Laplacians with normal boundary conditions as their spectra cover the reduced spectral sets. The models we test are the solid cube, ball, torus, and a spherical shell (a ball with a round cavity inside) with one model per each Laplacian. Additional figures are in the supplemental materials. We chose these shapes because they provide examples with trivial and nontrivial homology groups, and their exact solutions are available except for the torus. The Eulerian method performs competitively as opposed to the Lagrangian meshed-based evaluation. The BIG Laplacian, which we extended to handle both boundary conditions, differs from the corresponding Hodge Laplacian only near the boundary in the Cartesian grid. However, our computations demonstrate that the thin layer of difference introduces a great accuracy gain for the Hodge Laplacian.

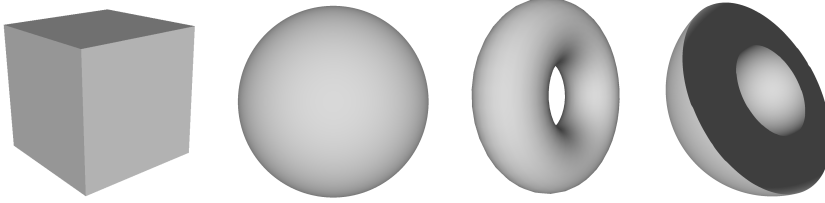


FIG. 5. 3D models used in Section 5.2 and the supplementary material. From left to right a cube, ball, torus, and a cut open spherical shell.

5.2.1. Scalar Laplacian under Dirichlet Boundary Condition $L_{0,n}$. We compared the spectra of three different discrete Laplacian matrices for scalar fields that vanish on the domain boundary, the Cartesian grid Hodge Laplacian, the BIG Laplacian modified for this boundary condition, and the Hodge Laplacian for a Lagrangian domain discretization, i.e., tetrahedral meshes assuming finite linear elements from [28]. The exact spectra of the continuous Laplacian operators for the cube, the ball, and the spherical shell are given in the supplementary material. For comparisons, we rescale the spectrum from the BIG Laplacian by $1/l_g^2$ as the BIG Laplacian is unitless, but the actual Laplacian carries a unit of one over length squared.

The kernel size of this Laplacian is 0 as it corresponds to the 0th relative homology with respect to the boundary. Equivalently, it is isomorphic to the kernel of $L_{3,t}$, which has a dimension equaling the Betti number $\beta_3 = 0$. Another way to interpret this is that the Laplace equation $\Delta f = 0$ on the domain M has a unique solution $f = 0$ under the Dirichlet boundary condition $f|_{\partial M} = 0$.

For the unit cube in Figure 6, we see that the Eulerian Hodge Laplacian is the closest to the exact solution, whereas the BIG Laplacian is the furthest away. We speculate that the better accuracy of the Eulerian Hodge Laplacian compared to the Lagrangian Hodge Laplacian is due to the better alignment of the Cartesian grid with this particular shape. Note that the Lagrangian mesh with a similar resolution requires more DoFs for the scalar field and the Lagrangian Laplacian operator is a denser matrix. The BIG and Hodge Laplacians share the same sparse structure on the grid and are localized to the thin boundary region. However, this small correction to the Hodge star leads to a substantial gain in accuracy.

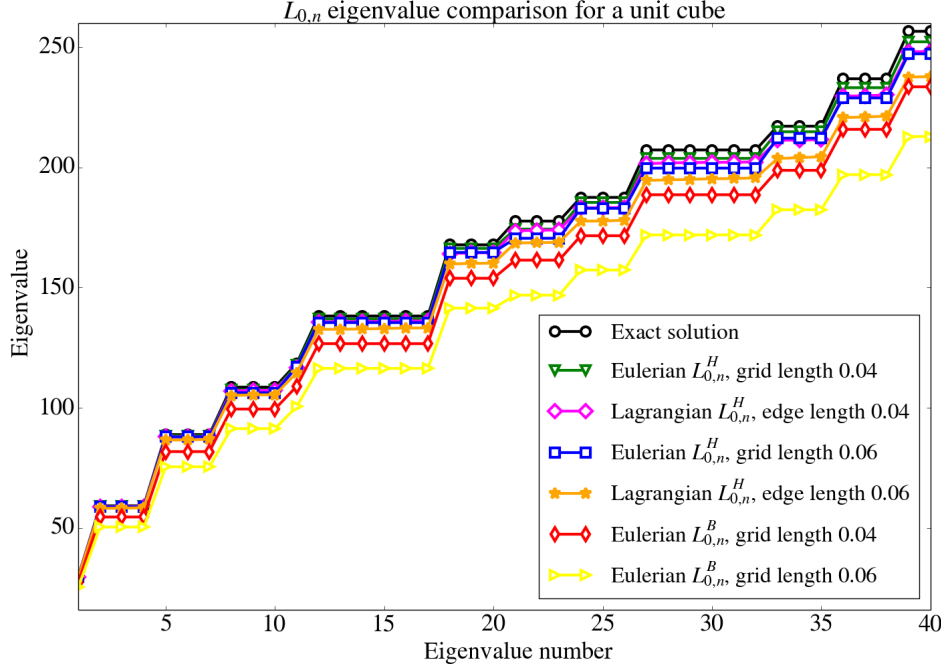


FIG. 6. The first 40 eigenvalues of $L_{0,n}$ for the unit cube. The exact solution, Eulerian BIG, and Hodge Laplacians are shown as well as the Lagrangian Hodge Laplacians from [28] for two different grid/edge lengths, 0.06 and 0.04.

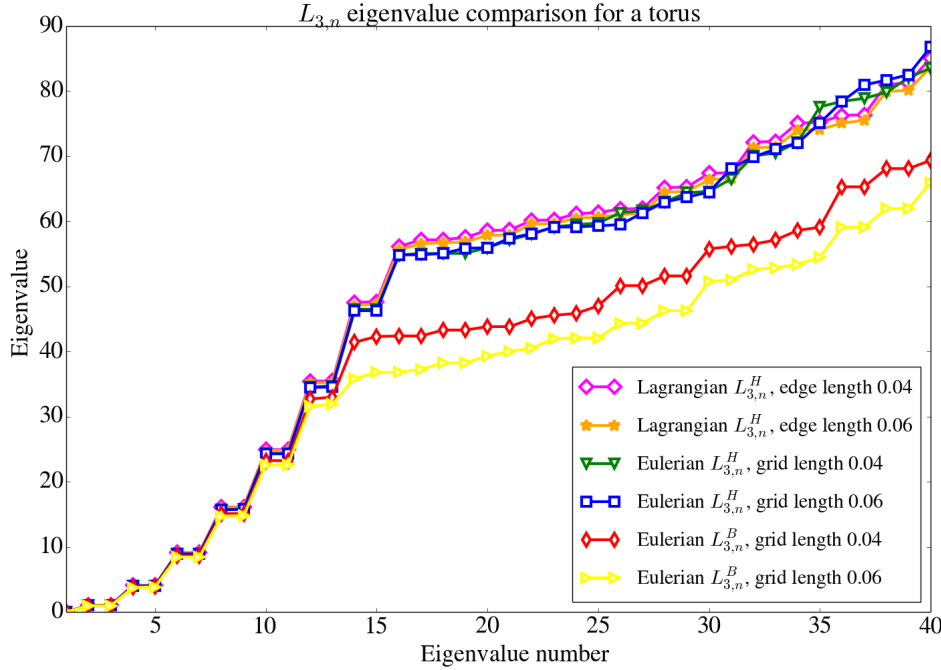


FIG. 7. The first 40 eigenvalues of $L_{3,n}$ for a torus. The Eulerian BIG and Hodge Laplacians are shown as well as the Lagrangian Hodge Laplacians from [28] for two different grid/edge lengths, 0.06 and 0.04. No exact solution was computed for the torus.

5.2.2. Scalar Laplacian under Neumann Boundary Condition $L_{3,n}$. We compared the spectra of two different discrete Laplacian matrices for scalar fields that have a 0 normal derivative on the domain boundary. The exact spectra of the continuous Laplacian operator for the ball and other models are given in the supplementary materials. The kernel size of this Laplacian corresponds to the dimension of the 3rd relative homology with respect to the boundary, or equivalently, the 0th homology, i.e., the number of connected components β_0 . We can also see that a constant scalar field is the only one satisfying the condition, which is still true with the discrete Hodge or BIG Laplacians. As expected and shown in Figure 7, the graph version consistently produces an accuracy far worse than the lower resolution results of the Hodge versions. Nevertheless, the kernel sizes (topological invariants) are correct. The other models are included in the supplementary material.

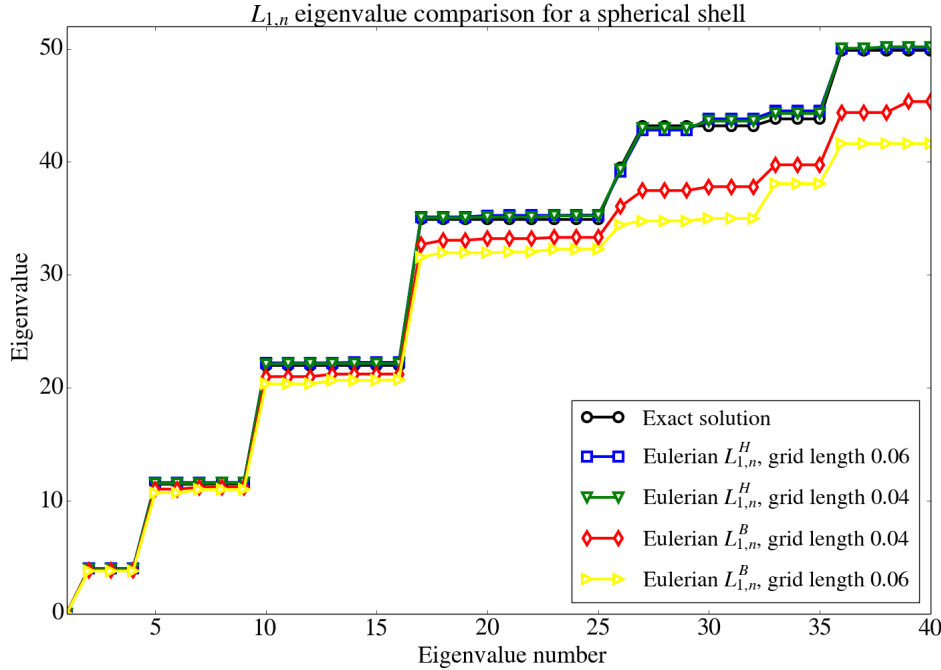


FIG. 8. The first 40 eigenvalues for $L_{1,n}$ for a spherical shell with outer radius 1.0 and inner radius 0.5. The exact solution, Eulerian BIG, and Hodge Laplacians are shown for two different grid edge lengths, 0.06 and 0.04.

5.2.3. Vector Laplacian under Normal Boundary Condition $L_{1,n}$. In the test for the Laplacian of vector fields that are normal to the domain boundary (along with the two Robin conditions to make the kernel finite), we found similar behaviors for the Laplacians as shown in Figure 8. The exact spectra of the continuous Laplacian operator for the spherical shell are again given in supplementary materials. The kernel size of this Laplacian corresponds to the dimension of the 1st relative homology with respect to the boundary, or equivalently, the 2nd homology, i.e., the number of cavities β_2 , of which the spherical shell has a nontrivial kernel. Our test confirms that both Hodge and BIG Laplacians do produce the right kernel. While this is the only nontrivial test, it can be explained by Algorithm. 3.1. Any k -cell is included whenever one of its vertices is inside, so if a dual cell is included, all its vertices, edges, and faces are included. Thus, the topology is the same as that of the voxelization of the

original shape on the dual grid, as long as the grid has a sufficiently fine resolution.

6. Concluding Remarks. Although both graph Laplacian and Hodge Laplacian can reveal the topological dimension and geometric shape of data, they are defined on discrete point cloud and continuous manifold, respectively. “Hodge Laplacian on graphs” [16] emphasizes graph Laplacian’s ability to implement differential vector calculus on graphs but is conceptually incompatible with Hodge Laplacian on manifolds with boundary. As a results, two approaches cannot be further compared. This work introduces Boundary-Induced Graph (BIG) Laplacian to bring graph Laplacian and Hodge Laplacian on an equal footing for detailed analysis and comparison. BIG Laplacians of various topological dimensions are defined on Cartesian domains with proper boundary conditions (i.e., Dirichlet and Neumann) to deliver the correct topological dimensions of data.

In the context of computing Betti numbers and the smallest eigenvalues, the BIG Laplacian may perform favorably and is simpler to compute, with proper modifications for boundary conditions. As shown, given uniform sampling, either a regular grid or uniform tetrahedral mesh, the spectra of BIG Laplacians have worse “accuracy” compared to the Hodge Laplacian spectra. However, if the input is irregularly sampled, which could be the case with real-world data, the Hodge star would be indispensable to account for nonuniform geometric quantities. The Hodge Laplacian preserves higher frequency spectral information, such as for shape and spectrum learning tasks. Furthermore, while the duality between normal and tangential boundary conditions indicates that the normal boundary condition of k -forms can be handled with the clique-based graph Laplacian for $(n-k)$ -forms, leading to correct kernel dimensions, only the correct boundary treatment through primal and dual grids can handle mixed boundary conditions, which are common in practical problems.

In practical applications, BIG Laplacians stand out as an independent formulation for the analysis of volumetric data, such as those from Cryo Electron Microscopy (Cryo EM), Magnetic Resonance Imaging (MRI), computer vision, and the solutions of Partial Differential Equations (PDEs). Its generalization to evolving manifolds, namely persistent BIG Laplacians (PBLs), in analogous to evolutionary de Rham-Hodge theory [4], will have much potential for machine learning modeling and prediction.

Code availability. BIG Laplacian code can be found at

<https://github.com/eribandogros/BIGLaplacians>.

Supplementary material. The Supplementary material is available for

- S1 Exact Laplacian spectra of elementary shapes
 - S1.1. Spectra of Laplacians on the unit ball
 - S1.2. Vector field Laplacian in spherical polar coordinates
 - S1.3. Spectrum of vector field Laplacian on ball
 - S1.4. Spectra on spherical shells
 - S1.5. Spectra on cuboids
- S2 Additional Results
 - S2.1. Planar Result
 - S2.2. 3D Results
 - S2.2.1. Scalar Laplacian under Dirichlet Boundary condition $L_{0,n}$
 - S2.2.2. Scalar Laplacian under Neumann Boundary condition $L_{3,n}$
 - S2.2.3. Vector Laplacian under Normal Boundary condition $L_{1,n}$

Acknowledgment. This work was supported in part by NSF grant IIS-1900473 and NIH grant GM126189.

REFERENCES

- [1] D. N. ARNOLD, *Finite Element Exterior Calculus*, Society for Industrial and Applied Mathematics, Philadelphia, PA, 2018, <https://doi.org/10.1137/1.9781611975543>, <https://epubs.siam.org/doi/abs/10.1137/1.9781611975543>, <https://arxiv.org/abs/https://epubs.siam.org/doi/pdf/10.1137/1.9781611975543>.
- [2] A. BOSSAVIT, *Computational electromagnetism and geometry : (5):the "galerkin hodge"*, Applied and Environmental Microbiology, 8 (2000), pp. 203–209.
- [3] M. M. BRONSTEIN, J. BRUNA, Y. LECUN, A. SZLAM, AND P. VANDERGHEYNST, *Geometric deep learning: going beyond euclidean data*, CoRR, abs/1611.08097 (2016), <http://arxiv.org/abs/1611.08097>, <https://arxiv.org/abs/1611.08097>.
- [4] J. CHEN, R. ZHAO, Y. TONG, AND G.-W. WEI, *Evolutionary de rham-hodge method*, Discrete and Continuous Dynamical Systems - B, 26 (2021), pp. 3785–3821.
- [5] F. R. CHUNG AND F. C. GRAHAM, *Spectral graph theory*, American Mathematical Soc., 1997.
- [6] B. DELAUNAY ET AL., *Sur la sphere vide*, Izv. Akad. Nauk SSSR, Otdelenie Matematicheskii i Estestvennyka Nauk, 7 (1934), pp. 1–2.
- [7] M. DESBRUN, E. KANSO, AND Y. TONG, *Discrete differential forms for computational modeling*, in ACM SIGGRAPH 2006 Courses, SIGGRAPH '06, New York, NY, USA, 2006, Association for Computing Machinery, pp. 39–54, <https://doi.org/10.1145/1185657.1185665>, <https://doi.org/10.1145/1185657.1185665>.
- [8] F. DORFLER AND F. BULLO, *Kron reduction of graphs with applications to electrical networks*, IEEE Transactions on Circuits and Systems I: Regular Papers, 60 (2013), pp. 150–163, <https://doi.org/10.1109/TCSI.2012.2215780>.
- [9] H. EDELSBRUNNER, J. HARER, ET AL., *Persistent homology-a survey*, Contemporary mathematics, 453 (2008), pp. 257–282.
- [10] W. C. FORSMAN, *Graph theory and the statistics and dynamics of polymer chains*, The Journal of Chemical Physics, 65 (1976), pp. 4111–4115, <https://doi.org/10.1063/1.432866>, <https://doi.org/10.1063/1.432866>, <https://arxiv.org/abs/https://doi.org/10.1063/1.432866>.
- [11] R. GHRIST AND H. RIESS, *Cellular sheaves of lattices and the tarski laplacian*, arXiv preprint arXiv:2007.04099, (2020).
- [12] T. E. GOLDBERG, *Combinatorial laplacians of simplicial complexes*, Senior Thesis, Bard College, (2002).
- [13] D. HORAK AND J. JOST, *Spectra of combinatorial laplace operators on simplicial complexes*, Advances in Mathematics, 244 (2013), pp. 303–336.
- [14] M. KAC, *Can one hear the shape of a drum?*, The American Mathematical Monthly, 73 (1966), pp. 1–23, <http://www.jstor.org/stable/2313748>.
- [15] H. LEE, M. K. CHUNG, H. CHOI, H. KANG, S. HA, Y. K. KIM, AND D. S. LEE, *Harmonic holes as the submodules of brain network and network dissimilarity*, in CTIC, 2019.
- [16] L. LIM, *Hodge laplacians on graphs*, CoRR, abs/1507.05379 (2015), <http://arxiv.org/abs/1507.05379>, <https://arxiv.org/abs/1507.05379>.
- [17] B. LIU, G. MASON, J. HODGSON, Y. TONG, AND M. DESBRUN, *Model-reduced variational fluid simulation*, ACM Trans. Graph., 34 (2015), pp. 244:1–244:12, <https://doi.org/10.1145/2816795.2818130>, <http://doi.acm.org/10.1145/2816795.2818130>.
- [18] R. MARIN, A. RAMPINI, U. CASTELLANI, E. RODOLA, M. OVSJANIKOV, AND S. MELZI, *Spectral shape recovery and analysis via data-driven connections*, International Journal of Computer Vision, (2021), <https://doi.org/10.1007/s11263-021-01492-6>.
- [19] Z. MENG AND K. XIA, *Persistent spectral-based machine learning (perspect ml) for protein-ligand binding affinity prediction*, Science Advances, 7 (2021), p. eabc5329.
- [20] R. MERRIS, *A survey of graph laplacians*, Linear and Multilinear Algebra, 39 (1995), pp. 19–31.
- [21] B. MOHAR, Y. ALAVI, G. CHARTRAND, AND O. OELLERMANN, *The laplacian spectrum of graphs*, Graph theory, combinatorics, and applications, 2 (1991), p. 12.
- [22] D. D. NGUYEN AND G.-W. WEI, *Agl-score: algebraic graph learning score for protein-ligand binding scoring, ranking, docking, and screening*, Journal of chemical information and modeling, 59 (2019), pp. 3291–3304.
- [23] S. REN, C. WANG, C. WU, AND J. WU, *On the discrete morse functions for hypergraphs*, arXiv preprint arXiv:2108.02384, (2021).
- [24] G. VORONOI, *Nouvelles applications des paramètres continus à la théorie des formes quadratiques. premier mémoire. sur quelques propriétés des formes quadratiques positives par-*

- faites.*, Journal für die reine und angewandte Mathematik, 1908 (1908), pp. 97–102.
- [25] R. WANG, D. D. NGUYEN, AND G.-W. WEI, *Persistent spectral graph*, International journal for numerical methods in biomedical engineering, 36 (2020), pp. e3376–e3376.
 - [26] Q. XU, Q. HUANG, T. JIANG, B. YAN, W. LIN, AND Y. YAO, *Hodgerank on random graphs for subjective video quality assessment*, IEEE Transactions on Multimedia, 14 (2012), pp. 844–857, <https://doi.org/10.1109/TMM.2012.2190924>.
 - [27] R. ZHAO, M. DESBRUN, G.-W. WEI, AND Y. TONG, *3d hodge decompositions of edge-and face-based vector fields*, ACM Transactions on Graphics (TOG), 38 (2019), pp. 1–13.
 - [28] R. ZHAO, M. WANG, J. CHEN, Y. TONG, AND G.-W. WEI, *The de rham–hodge analysis and modeling of biomolecules*, Bulletin of mathematical biology, 82 (2020), pp. 1–38.
 - [29] A. ZOMORODIAN AND G. CARLSSON, *Computing persistent homology*, Discrete & Computational Geometry, 33 (2005), pp. 249–274.